Unsupervised Geometrical Feature Learning from Hyperspectral Data

Muhammad Ahmad, Adil Mehmood Khan,
Rasheed Hussain, and Stanislav Protasov
Innopolis University, Innopolis, Russia
E.mail: {m.ahmad, a.khan, r.hussain,
s.protasov}@innopolis.ru

Francis Chow[1], and Asad Masood Khattak[2]
[1]University College
[2]College of Technological Innovation
Zayed University, UAE
E.mail: {francis.chow, asad.khattak}@zu.ac.ae

Abstract—**Hyperspectral technology has made significant advancements in the past two decades. Current sensors onboard airborne and space-borne platforms cover large areas of the Earth surface with unprecedented spectral resolutions. These characteristics enable a myriad of applications requiring fine identification of materials. Quite often, these applications rely on complicated methods of data analysis. In essence, the challenges include high dimensionality, spectral mixing, and atmospheric effects. This paper presents a robust unsupervised method to efficiently overcome this issue. The proposed algorithm performs three core tasks to acquire good results: i) optimizing the weights within a fixed threshold value for pure pixel estimation, ii) finding the best-averaged weighted endmember signatures with similarity error below the threshold value, and iii) iterating until a fixed number of average weighted endmembers is chosen. The experimental results on both real and synthetic data demonstrate that the proposed method is more robust and accurate then other geometrical methods.**

Keywords—Unsupervised Hyperspectral unmixing, Endmembers, Geometry of affine transformation, Peter Gustav Lejeune dirichlet distribution

I. INTRODUCTION

HYPERSPECTRAL remote sensing is concerned with the extraction of information from objects from the Earth's surface, based on their radiance acquired by airborne or space-borne sensors [1, 2]. HS imaging has been increasingly used in real life applications such as food safety, pharmaceutical process monitoring and quality control, biomedical, industrial, and biometric. The signal recorded by a hyperspectral sensor of a given image and from a given pixel, setting aside the effects of the atmosphere, is a mixture of the light scattered by the constituent substances located in the respective pixel coverage. There are two different types of mixing: i) linear mixing in a checkerboard type surface, and ii) nonlinear mixing in an intimate/particulate media. Therefore, when mixing occurs, it is no longer possible to determine what materials are present in the pixels directly from the respective measured spectral vectors. More precisely, the key feature of spectral sensors, which is their ability to discriminate materials based on their spectral responses, is compromised.

With the objective of recovering the ability to discriminate the materials, a handsome amount of research has been devoted to hyperspectral unmixing [3]. We consider a linear mixing scenario. Linear mixing holds true when the mixing scale is macroscopic and the incident light interacts with just one material. As a result, the light from the materials, though almost completely separated, is linearly mixed within the measuring instrument, owing to insufficient spatial resolution. Inspired by the linear mixing models, the hyperspectral unmixing problem is very often defined as unsupervised estimation of the endmembers.

The linear mixing model has been widely used to address hyperspectral unmixing problems. The reason is three-fold: i) despite its simplicity, the linear mixing model is an acceptable approximation for the light scattering in many real scenarios. ii) Linear mixing model yields well-posed inverse problems and iii) under the linear mixing models, hyperspectral unmixing is interpretable as blind source separation [4], non-negative matrix factorization [5, 6], and geometric problems [7, 8, 9] that have been vastly researched in many signal processing areas. These methods assume the presence of at least one pure pixel per endmember, meaning that there is at least one spectral vector on each vertex of the data simplex, which is difficult to guarantee, because this assumption might yield a virtual pixel with no physical meaning [10]. Generally, in geometrical approaches, the reflections from an image are in a simplex whose vertices coincide in their characteristics to an endmember. Several versatile approaches [11-13] have exploited this geometric feature of hyperspectral mixtures, and aiming at lower computational complexity, some of them find the minimum volume simplex, but again they assume presence of at least one pure pixel, which is an invulnerable requisite that may not hold in some datasets. Furthermore, the minimum volume transformation type approaches are complex from a computational point of view. Beside geometric approaches, sparse unmixing approaches have also been proposed [14-19], and they do not need to extract the endmembers from hyperspectral data. In recent years, more efforts have been made to incorporate the spatial contextual information [20-22], and subspace nature approaches [23-25] to obtain better results.

The use of prior knowledge for unmixing is a common practice in many areas of computer science, such a brain-computer interface [26]. To improve the unmixing accuracy, this work also uses the characteristics or prior knowledge

concerned with hyperspectral data into the unmixing framework. Recently as more libraries have become openly available, unsupervised approaches that take the spectral vectors as prior knowledge have been proposed to address the problem concerning the virtual endmembers [27-29]. Almost all the discussed approaches have their own advantages and disadvantages, but all have one common shortcoming of random assumption of pure pixels that might lead to high similarity error rate while having noise and topographic effects.

Our proposed scheme will overcome the limitations of random selection of pure pixels, in which the weights are updated by using gradient decent type method. The proposed algorithm exploits two major facts: i) the average weighted endmembers are the vertices of simplex and ii) the geometry of affine transformation of simplex is also simplex. The proposed scheme iteratively projects the data onto the direction orthogonal to the full space initialized by the acquired pure pixels. The new endmembers signatures correspond to the extreme of the projection and iterate until the fixed number of endmembers are chosen. The main contributions of our proposed algorithm are: i) optimizing the weights within a fixed threshold value for pure pixel estimation, ii) finding the best-averaged weighted endmember signatures with similarity error below the threshold value, and iii) iterating until a fixed number of average weighted endmembers is chosen. The proposed scheme works with both projected and un-projected data. We also fix the pure pixels for every experiment within single execution to minimize the similarity error. The proposed work is an extension to the work presented in [7] with profound improvements in terms of unmixing performance and computational cost, and we successfully overcome the problem of random assumption for pure pixels.

The rest of the paper is structured as follows. Section II describes the materials and methods. Section III evaluates the proposed algorithm and finally section IV presents the concluding remarks.

II. MATERIAL AND METHODS

Under the LM models, a given measured hyperspectral vector can be written as

$$R = X + W = Ms + W \qquad (i)$$

where R is an $L * N$ dimensional matrix, and L and N are the number of band images and pixels respectively, $M = [m_1, m_2, m_3, ..., m_p]$ is the mixing matrix, and p is the number of endmembers and $s = [s_1, s_2, s_3, ..., s_p]^T = \gamma \alpha^T$, where γ is a scale factor and α^T stands for fractional abundances, and finally W accounts for additive perturbations due to model mismatches and additive noise. The components of α represent abundance fractions that satisfy the constraints of non-negativity and constant sum as;

$$\alpha_i \geq 0$$

$$\sum_i \alpha_i = 1, \qquad where\ i = 1,2,3, ..., p$$

Let $\{\alpha \in \Re^L : \alpha \geq 0\}$ be a simplex so $s_X = \{X \in \Re^L : X = M\gamma\alpha\}$ is also simplex and $s_p = \{Y \in \Re^L : Y = $

$\frac{R}{R^T u}, R \in T_p\}$ is the projective projection of the convex cone T_p onto the plane $R^T u = 1$, where the choice of u assures that there is no observed vectors orthogonal to it. In such a scenario, the proposed algorithm iteratively projects the data in the direction orthogonal to the space spanned by the endmembers and the new endmembers spectra correspond to the extreme of the projection. After the first projection, spectral vectors are estimated in new p-dimensional space and later projected back onto the entire space. Furthermore, we know that $p \ll L$, and this leads to a significant decrease in computational complexity in terms of time and memory.

Later the algorithm identifies L_p by singular value decomposition (SVD) in the presence of noise and then projects the points in L_p onto a simplex s_p by computing $Y = \frac{R}{R^T u}$. This simplex is contained in an affine set of dimension $p - 1$. We note that the algorithm is still valid if the observed data is projected onto space L_d, which is a super-space of L_p of dimension d, where $p \leq d \leq L$, i.e., the projection of the cone L_p onto L_d followed by a projection is also a simplex with the same vertices. The complete process is explained in algorithm 1.

Algorithm 1: $Input: dmin, dmax, R, w, (\#^T transpose)$

$for\ i = 1:t$

    $for\ j = 1:k$

1. $X = U_d^T R$, $where\ U_d\ is\ incurred\ by\ SVD, d = k$

2. $[Y]_{:,j} = \left(\frac{[X]_{:,j}}{[X]_{:,j}^T \mu} \right)$, $where\ \mu\ is\ mean(X)$

3. $[X]_{:,j} = U_d^T([R]_{:,j} - \mu)$, $where\ d = k - 1$

4. $a = \underset{j = 1, ... N}{argmax} \| [X]_{:,j} \|$

    $if\ i = 1$

5. $w = (dmin - dmax) * w(k, 1) + dmin$

    $else$

6. $dmin^i = dmin^{t-1} + \lambda^t \left(\frac{\partial w}{\partial dmin^{t-1}} \right)^T$

    $dmax^i = dmax^{t-1} + \lambda^t \left(\frac{\partial w}{\partial dmax^{t-1}} \right)^T$

7. $w^i = (dmin^i - dmax^i) * w + dmin$

    $end\ if$

8. $s_k = \frac{(I - Aux * Aux^T)w}{\|(I - Aux * Aux^T)w^i\|}$

9. $v = d_k^T Y$

10. $p^i = \underset{j = 1, ... N}{argmax} \| [v]_{:,j} \|$

11. $[Aux]_{:,p} = [Y]_{:,p}$

12. $[indice]_i = p$

    $end\ for$

13. $M = U_d[X]_{:,indice} + \mu$

14. $s = pinv(M)R$

    $if\ i = 1$

15. $M = M$

    $s = s$

    $else$

16. $M = t \dfrac{dist(M^{i-1}, M^i)}{\|M^{i-1}\|\|M^i\|}$

    $s = t \dfrac{dist(s^{i-1}, s^i)}{\|s^{i-1}\|\|s^i\|}$

17. $M \to M^i$

    $s \to s^i$

    $end\ if$

$end\ for$

18. $\varphi = cos^{-1}\left[\dfrac{(M_{estimated}, M_{actual})}{\|M_{estimated}\|\|M_{actual}\|}\right]$

    $\omega = cos^{-1}\left[\dfrac{(s_{estimated}, s_{actual})}{\|s_{estimated}\|\|s_{actual}\|}\right]$

19. $SAE = \left(\dfrac{1}{t} E[\|\varphi_i\|_2^2]\right)^{\frac{1}{2}}$

    $AAE = \left(\dfrac{1}{t} E[\|\omega_i\|_2^2]\right)^{\frac{1}{2}}$

Steps 1 to 3 assure that the inner product between $[X]_{:,j}$ and μ is non-negative, and step 4 assures that the colatitudes angle of μ and $[X]_{:,j}$ is between 0^0 and 45^0 . Steps 5 to 7 are an optimization problem, which we solve by using the fact that the w is a non-decreasing function. Steps 8 to 12 find the number of endmembers and the extreme projection for each endmember.

Step 13 stores the projection of estimated average weighted endmember signatures. It is assumed that there exists at least one pure pixel of each endmember in the input sample R, which is further investigated through iterative process. The first time loop is executed: a vector s_p orthonormal to the space spanned by the columns of the auxiliary matrix is randomly generated, and Y is projected onto s_p. Since we assume that pure pixels occupy the vertices of a simplex, thus $a \le s_p^T[Y]_{:,j} \le b, j = 1,2,3,\dots,N$, where a and b correspond only to pure pixels. We store the endmember signatures corresponding to $max(|a,b|)$. In the next loop, s_p is orthogonal to the space spanned by the signatures that are already determined in first loop. Since s_p is the projection of a zero-mean white Gaussian independent random vector onto the orthogonal space spanned by the columns of $[X]_{:,j}$,the probability of s_p being null is zero.

Finally, steps 13 to 17 compute M and s, which contain the estimated endmember signatures and their abundance fractions. This process continues until we get the maximum averaged

pure endmembers. We execute this process multiple times and calculate the average, which produces better results when compared with the first attempt.

To evaluate the performance of the proposed method, we compute the angles in step 18. We also compute the error by an entropy-based distance to compare the similarity between estimated and actual endmember signatures. We compute these distances in step 19, which is also important to set a valid threshold for similarity angle measurement, where SAE stands for spectral angle error and AAE stands for abundance angle error.

III. EVALUTION AND EXPERIMENTAL RESULTS

This section describes the evaluation of the proposed method on real and synthetic data.

A. Evaluation with Synthetic Data

The experiments of this section are based on simulated scene, in which we know the spectra of each endmember. In all these experiments, the spectral signatures are selected from United States Geological Survey Library (*USGS library*) [30]. By this process, we aim to conclude that the proposed method works well and can extract more spectral signatures from hyperspectral data than from other geometrical methods with maximum similarity.

For the purposes of illustration, a simulated scene was generated according to equation (i). To show the performance of proposed method, we used a different number of pixels for synthetic data (*122500, 50176, and 10000*) with different number of endmembers (*3, 5 and 25*). There is no such restriction to generate the number of pixels and consider number of endmembers to generate the synthetic data.

The process to generate synthetic data is explained in algorithm 2, in which we include the different number of endmember signatures that were randomly selected from USGS library. We also consider that the abundance fractions follow the dirichlet distribution, and the noise is zero-mean white Gaussian with covariance matrix $\sigma^2 I$. Clearly, here our focus is not to reduce the noise variations or its estimation; noise is considered for leading to a visible improvement on the results.

Algorithm 2: $Input\ p, n, N, SNR, M, L$

1. $B = random\ variables\ with\ Gamma\ Distribution$

2. $s = Generate\ dirichlet\ distribution$

3. $X = M * Trans(s), (Linear\ Mixture\ System)$

4. $Ver = mean(X^T * X)/\left(\left(10^{\frac{SNR}{10}}\right)/L/N\right)$

$if\ White\ Noise$

5. $Ver\_X = Ver * L * n$

6. $NC = Diag(Ver\_X)$

7. $N = (NC)^{\frac{1}{2}}rand([LN])$

$if\ Poisson\ Noise$

8. $F = \frac{Ver}{mean(X)}$

9. $N = (F)^{\frac{1}{2}}(X)^{\frac{1}{2}}rand([LN])$

end if

10. $R = X + N$

In total, we performed five experiments. In our first experiment, we evaluate the proposed strategy with respect to signal to noise ratio (SNR) and to absence of pure pixel, which will later update the pure pixels by iterative fashion in extreme projection. The noise is zero-mean white Gaussian with covariance and dirichlet abundance fractions as explained in algorithm 2. In this experiment, the hyperspectral data has 122500 pixels and the abundance fractions are dirichlet distribution with $\tau_1 = \tau_2 = \tau_3 = \tau_4 = \tau_5 = \frac{1}{3}$. Table I shows the performance results as the function of SNR, and as expected, the presence of noise did not affect the performance. In terms of SAE and AAE, we can see that when SNR is less than 30 db, the proposed model exhibits the best performance and almost attain zero SAE even in the presence of noise.

TABLE I. ERROR MEASUREMENTS ACCORDING TO THE VARIATIONS OF SNR WITH $N = 122500$ NUMBER OF PIXELS, $L = 224$ BANDS, AND $P = 5$ NUMBER OF ENDMEMBERS

	SAE		
	SNR 30 db	**SNR 20 db**	**SNR 10 db**
Endmember 1	0.001216	0.005154	0.009806
Endmember 2	0.001877	0.005008	0.003977
Endmember 3	0.001281	0.005901	0.004575
Endmember 4	0.001409	0.008136	0.003876
Endmember 5	0.002820	0.011067	0.005345
	AAE		
Endmember 1	0.001246	0.003577	0.001919
Endmember 2	0.001306	0.003333	0.002320
Endmember 3	0.001164	0.002780	0.001974
Endmember 4	0.001648	0.002774	0.002812
Endmember 5	0.002985	0.003115	0.002208

In the second experiment, the number of pixels of the scene varies in order to illustrate the performance with the size the covered area. As the number of pixels increases, the probability of having pure pixels also increases. The abundance fractions are generated similarly to the first experiment and $SNR = 30\ db$. The variations of different number of pixels on performance are presented in Table II. We observe that SAE and AAE disclose similar behavior; therefore, in remaining experiments we will only consider SAE.

TABLE II. ERROR MEASUREMENTS ACCORDING TO THE NUMBER OF PIXLES WITH $L = 224$ BANDS, $P = 5$ NUMERB OF ENDMEMBERS, AND $SNR = 30db$

	SAE		
	N = 122500	**N = 50176**	**N = 10000**
Endmember 1	0.001216	0.005967	0.001550
Endmember 2	0.001877	0.007778	0.001525
Endmember 3	0.001281	0.008665	0.003836
Endmember 4	0.001409	0.005790	0.002873
Endmember 5	0.002820	0.009033	0.001472
	AAE		
Endmember 1	0.001246	0.001083	0.001200

Endmember 2	0.001306	0.001184	0.001572
Endmember 3	0.001164	0.001088	0.002103
Endmember 4	0.001648	0.001563	0.001175
Endmember 5	0.002985	0.000960	0.001267

In the third experiment, the performance is measured as a function of the parameter γ, which models fluctuations on the illumination due to the surface topography. In this experiment, the abundance fractions were generated similar to the first experiment and SNR varies from 10 db to 30 db. The beta function parameters are $(2,28)$. This corresponds to varying $E[\gamma]$ within the range of $(0.66{\sim}0.96)$ and σ_γ ranges from $(0.23{\sim}0.03)$. By varying the first parameter of beta function, the severity of topographic modulation is also varied, which explains the effect of topographic modulation on the performance of the algorithm, and when beta grows, the performance improves with respect to the smaller values of σ_γ. The said effects were expected because simplex identifications are more accurate when the topographic modulations are smaller. Thus, the said model has the best performance and is more robust to topographic modulation.

In the fourth experiment, the algorithm is evaluated as a function of the number of endmembers presented in the scene. In this experiment, we vary the number of endmember signatures from $p = 3\ to\ p = 25$, the scene has $N = 122500$ pixels and $SNR = 30\ db$. The SAE is almost better on the increment of the number of endmembers. We also conclude one major improvement that the performance increases in average as the number of endmembers increases. Figure 1 shows the performance of proposed strategy and vertex component analysis (VCA), where the proposed strategy performed better than VCA [7] in average.
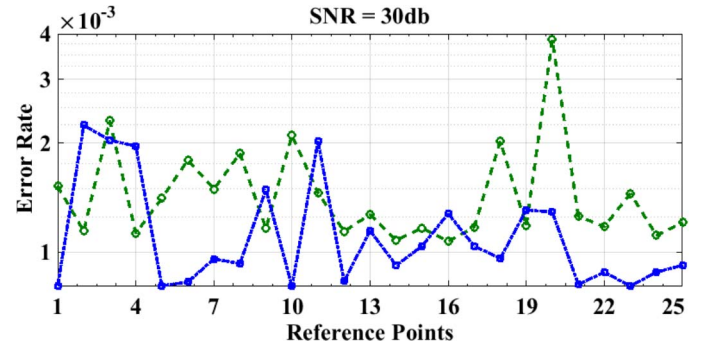
Figure 1: Spectral Signature angle error comparison between the proposed strategy and original VCA. The number of endmembers are 25, pixels are 122500. Green line represents the SAE obtained by VCA corresponds to each endmember, and Blue line shows the proposed strategy for each endmember.

The results presented in this experiment are based on the abundance fractions with symmetric dirichlet distribution. The relative performance of two algorithms is shown in Figure 1. We can conclude that the performance of VCA varies according to the noise power and number of endmembers, but the performance of proposed method is much better with more endmembers and with no effect of SNR at all. Both process have similar atmospheric correction effects, but on average are lower than in the proposed method.

Finally, in the fifth experiment, the number of floating points operations is measured in order to compare the computational complexity of the proposed model. In this experiment, the number of endmembers is measured in order to compare the computational complexity. Herein, we use the scenarios of the second and third experiments. We present an approximated expression $O(N)$ for the number of endmembers used by the proposed strategy with and without considering the computational complexities involved in the computations of Eigen decompositions and covariance computations. Since covariance and Eigen decompositions have $2NL^2$ power for full hyperspectral data, the computational cost is $2p^t(NL)^2$. The computational cost without covariance and Eigen decomposition is p^tN.

B. Evaluation with Real Data

In this section, we apply the proposed strategy to real hyperspectral data collected by Airborne Visible / Infrared Imaging Spectrometer ($AVIRIS$) sensor over Cuprite NV. Cuprite is a mining area in southern Nevada with mineral and little vegetation, located approximately $200\ KM$ northwest of Las Vegas. A geologic summary and a mineral map can be found in [31-32].

The presented work based on 350*350 pixels of data acquired by the AVIRIS flight June 19, 1997. The instrument of AVIRIS covers $0.41\sim2.45\ \mu m$ regions in 224 spectral band images with a $10\ nm$ bandwidth and flying at an altitude of $20Km$. It has as instantaneous Field of View of $20\ m$ and views a swath over $10\ Km$ wide. Prior to the analysis of AVIRIS Cuprite data, low SNR spectral band images $1\sim3, 105\sim115$, and $150\sim170$ have been removed and 189 band images were used for experiment. In order to compare the results with library spectral signatures, we process the reflectance image after atmospheric correction.

In order to confirm the classification based on the abundance fractions, a comparison of the estimated endmembers spectra with laboratory endmembers spectra is presented in Figure 2 and Figure 3. The estimated spectral signatures are close to the library spectral signatures within a specific threshold of similarity error. Those that are above the similarity error threshold are highlighted in red in Figure 3. We randomly selected 25 endmembers for each experiment and compared them with the same extracted spectral signatures in the second experiments of this section. In both experiments, the similarity among the found and the actual spectral signatures are presented in Figure 2 and Figure 3, which show the performance and efficiency of the proposed strategy for hyperspectral unmixing in noisy environment. The mid-range of each found spectral value in Figure 2 has some distortion because of the additive noise.
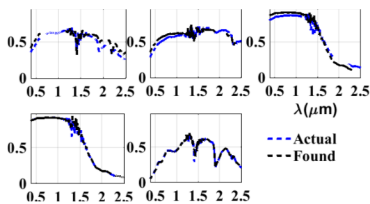

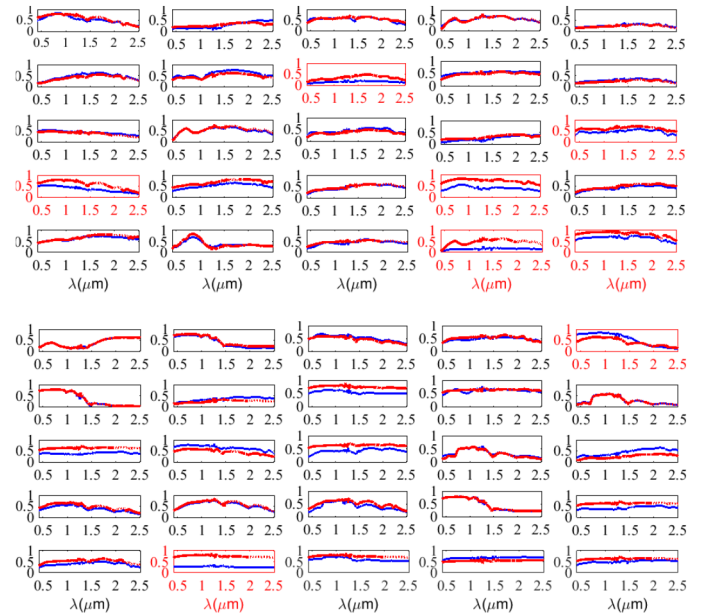**Figure 2:** Similarity among actual and found spectral signatures

Figure 3: (A-B): Comparison of the extracted signatures (doted lines-Red) with the USGS (solid lines-Blue). 25 signatures were random selected form USGS spectral library, and compared with the extracted spectra's. We recoded higher similarities in average expect the ones highlighted in red.

IV. DISCUSSION AND CONCLUSION

In this paper, we have investigated an average weighted unmixing procedure. The proposed scheme is unsupervised, which is based not only on the geometry of a convex set, but also on a weighted average of spectral signatures. In this process, the assumption of the presence of pure pixels is relaxed, and it iteratively updates the randomly selected pixel until the pure pixel turns out. The extracted averaged endmember signature from projected space corresponds to the extreme of the projection. We then fix the pure pixel in each experiment for all executions and analyze the optimization behavior for similarity error. A fixed number of endmembers is extracted in an iterative fashion within the minimum similarity error in all executions.

The proposed algorithm profiling size is $1.38\ GB$ in total. The total CPU time elapsed for generating hyperspectral data with $L = 224$, $N = 122500$, $p = 25$, $SNR = 30\ db$ and additive noise is 21.312514 seconds, and the CPU time elapsed for unmixing with projection computations using singular value decomposition (SVD) is approximately 4.867138 seconds. The total CPU time for single execution is 26.180345 seconds. The CPU time mentioned above is the total time of execution, not self-time. Self-time is the time spent in a function excluding the time spent in its child functions. Self-time also includes overhead resulting from the process of profiling. The self-time for data generating is 12.827 seconds only.

Several experiments with simulated data lead to the conclusion that the proposed strategy performs exceptionally in the presence of noise and in higher order of endmembers extraction. This conclusion has great impact when the dataset has a large number of noisy pixels.

REFERENCES

[1] G. Camps-Valls, et al, Remote Sensing Image Processing. San Rafael, CA: Morgan and Claypool, 2011.

[2] M. Ahmad et al, "Blind Feature Selection and Extraction in 3-D image cube", Journal of Flow Visualization and Image Processing, vol. 19(2), pp. 97-111, 2012.

[3] J. B. Dias, et al, "Hyperspectral unmixing overview: Geometrical, statistical, and sparse regression-based approaches," IEEE Jouranl of Selected Topics on Applied Earth Observations and Remote Sensing, vol. 5(2), pp. 354–379, 2012.

[4] M. Berman, "Ice: A statistical approach to identifying endmembers in hyperSpectral images," IEEE Transactions on Geosciences and Remote Sensing, vol. 42(10), pp. 2085–2095, 2004.

[5] D. D. Lee, H. Sebastian Seung, "Learning the parts of objects by nonnegative matrix factorization", Nature, vol. 401, pp. 788–791, 1999.

[6] V. P. Paucaa, et al, "Nonnegative matrix factorization for spectral data analysis", Linear Algebra and its Applications, vol. 416(1), pp. 29–47, 2006.

[7] J. M. Nascimento, J. B. Dias, "Vertex component analysis: A fast algorithm to unmix hyperspectral data," IEEE Transactions on Geosciences and Remote Sensing, vol. 43(4), pp. 898–910, 2005.

[8] M. Ahmad, et al, "Hyperspectral remote sensing: Dimensional reduction and endmember extraction", International journal of soft computing and engineering, vol. 2 (2), pp. 170-175, 2012.

[9] M. Winter, "Fast autonomous spectral end member determination in hyperSpectral data," In Process of 13th International Conference on Applied Geological Remote Sensing, vol. 2, pp. 337–344, 1999.

[10] X. Chen, et al, "A quantitative analysis of virtual endmembers' increased impact on the co linearity effect in spectral unmixing," IEEE Transactions on Geosciences and Remote Sensing, vol. 49(8), pp. 2945–2956, 2011.

[11] Q. Mushtaq, et al, "Hyperspectral Blind unmixing and multiple target detection using linear mixture model, In proc. of 2nd ICKEM, Journal of Advanced Materials Research, vol. 488-489, pp. 1224-1228, 2011.

[12] M. Ahmad and I. U. Haq, "Hyperspectral unmixing using statistics of q function", In proc. of 7th ICMENS, Journal of Advanced Materials Research, Vol. 403-408, pp. 59-63, 2011.

[13] M. Ahmad and I. U. Haq, "Linear unmixing and target detection of hyperspectral imagery using OSP", In proc. of IPCSIT, vol.10, pp. 179-183, 2011.

[14] J. A. Tropp, "Computational methods for sparse solution of linear inverse problems," In Proceedings of the IEEE, vol. 98(6), pp. 948–958, 2010.

[15] M. Elad, "Sparse and Redundant Representations: From Theory to Applications in Signal and Image Processing", Book, Springer-Verlag, 2010.

[16] J. B. Dias, M. A. Figueiredo, "Alternating direction algorithms for constrained sparse regression: Application to hyperspectral unmixing," in Process of IEEE WHISPERS, pp. 1–4, 2010.

[17] K. E. Themelis, et al "A novel hierarchical Bayesian approach for sparse semi supervised hyperspectral unmixing," IEEE Transactions on Signal Process, vol. 60(2), pp. 585–599, 2012.

[18] F. Chen and Y. Zhang, "Sparse hyperspectral unmixing based on constrained Lp-L2, optimization," IEEE Transactions on Geosciences and Remote sensing Letters, vol. 10(5), pp. 1142–1146, 2013.

[19] W. Tang, Z. Shi, Z. Duren, "Sparse hyperspectral unmixing using an approximate l0 norm," Optik International Journal of Light Electron Optik, vol. 125(1), pp. 31–38, 2014.

[20] M.-D. Iordache, et al, "Total variation spatial regularization for sparse hyperspectral unmixing," IEEE Transactions on Geosciences and Remote sensing, vol. 50(11), pp. 4484–4502, 2012.

[21] X.-L. Zhao, et al,"De-blurring and sparse unmixing for hyperspectral images," IEEE Transactions on Geosciences and Remote sensing, vol. 51(7), pp. 4045–4058, 2013.

[22] W. Tang, et al, "Regularized simultaneous forward backward greedy algorithm for sparse unmixing of hyperspectral data." IEEE Transactions on Geosciences and Remote sensing, vol. 52(9), pp. 5271–5288, 2014.

[23] M. Ahmad, et al, "A new statistical approach for band clustering and band selection using K-Means clustering", International Journal of Engineering and Technology, vol. 3(6), pp. 606-614, 2011.

[24] M. D. Iordache, et al, "Collaborative sparse regression for hyperspectral unmixing," IEEE Transactions on Geosciences and Remote sensing, vol. 52(1), pp. 341–354, 2014.

[25] Z. Shi, et al, "Subspace matching pursuit for sparse unmixing of hyperspectral data," IEEE Transactions on Geosciences and Remote sensing, vol. 52(6), pp. 3256–3274, 2013.

[26] O. Idris Khan, at al, "Extraction of P300 using constrained independent component analysis", In proc. of IEEE Annual International Conference of the IEEE Engineering in Medicine and Biology Society, pp. 4031-4034, 2009.

[27] M. D. Iordache, et al, "Sparse unmixing of hyperspectral data," IEEE Transactions on Geosciences and Remote sensing, vol. 49(6), pp. 2014–2039, 2011.

[28] M. Ahmad, et al, "AIK method for band clustering using statistics of correlation and dispersion matrix", In proc. of IPCSIT, vol.16, pp. 114-118, 2011.

[29] J. B. Greer, "Sparse de-mixing of hyperspectral images," IEEE Transactions on Image Processing, vol. 21(1), pp. 219–228, 2012.

[30] R. N. Clark, et al, "The U.S. Geological Survey digital spectral library: Version 1: 0.2 to 3.0 μm", U.S. Geology Survey, Denver CO, Open File Rep. 93-592, 1993.

[31] R. Ashley, M. Abrams, "Alteration mapping using multispectral images-Cuprite Mining District, Esmeralda County", U.S. Geology Survey, Denver & CO, Open File Receipt 80-367, 1980.

[32] G. Swayze, "The hydrothermal and structural history of the Cuprite Mining District, southwestern Nevada: An integrated geological and geophysical approach", PhD dissertation, University of Colorado, 1997.